BBA - General Subjects 1869 (2025) 130803

Contents lists available at ScienceDirect

BBA - General Subjects

journal homepage: www.elsevier.com/locate/bbagen

Redox modulation via a synthetic thiol compound reshapes energy metabolism in endothelial cells and ameliorates angiogenic expression in a co-culture study with activated macrophages

Michela Bruschi *, Sofia Masini, Federica Biancucci, Giovanni Piersanti, Barbara Canonico, Michele Menotta, Mauro Magnani, Alessandra Fraternale

Department of Biomolecular Sciences, University of Urbino Carlo Bo, 61029 Urbino, PU, Italy

ARTICLE INFO

Keywords:
Metabolism
OXPHOS
ATP
Redox
Cysteine
Endothelial cells
Thiol

ABSTRACT

The vascular endothelium is the first interface exposed to circulating compounds and oxidative as well as pro-inflammatory *stimuli*. Nowadays, cysteine pro-drugs are emerging as new and potential therapies in cardiovascular and inflammatory diseases due to their cytoprotective effects. In this study, the effects of redox modulation by a synthetic thiol compound, i.e., I-152, a precursor of *N*-acetylcysteine (NAC) and cysteamine (MEA), were evaluated after 6 h and 24 h treatment on human umbilical cord endothelial cell (HUVECs) energy metabolism. Following I-152 treatment, higher cysteine and glutathione (GSH) content were detected via HPLC, in concomitance with I-152 derivatives, i.e., NAC and MEA. Untargeted metabolomics confirmed GSH upregulation and NAC presence in addition to I-152 itself and other metabolites, such as dithiol compound (NACMEAA) and triacetylated I-152. Mass spectrometry revealed that I-152 boosted ATP production, specifically through the mitochondrial OXPHOS, as determined via Seahorse assay without inducing oxidative stress. Additionally, I-152 treatment of HUVECs before co-culture with LPS-stimulated macrophages provided GSH and cysteine sustainment and attenuated the transcription of adhesion molecules as well as *iNOS* expression. Identifying the impact of redox regulation in physiological conditions and the possible metabolic targets could aid the application of novel thiol-based therapeutics.

1. Introduction

Endothelial cells (ECs) are ubiquitously present along the lumen walls. Being the interface between blood and the underlying tissues, they are involved in a broad array of functions, such as selective permeability of ions, macromolecules or signaling, maintenance of homeostasis with blood cell interactions, cross-talk with the immune system and formation of new blood vessels also known as angiogenesis [1–3]. Therefore, ECs are not merely inert vessel lining material, and due to their wide-ranging presence, they exhibit behavioral plasticity that allows them to adapt to several *stimuli*, for example, varying concentrations of oxygen and surface pressure [3–5].

However, a dysfunctional or pathological environment inducing oxidative stress may lead to redox alterations and reduced glutathione (GSH) depletion, resulting in mitochondrial injury or irreversible cellular damage [6,7]. GSH is one of the key factors in the antioxidant response, and its ratio over the oxidized form (GSSG), together with the redox couples $NAD(P)^+$ and NAD(P)H, contributes to redox homeostasis [8]. The amino acid cysteine (Cys) is a component of the tripeptide GSH in combination with glycine (Gly) and glutamate (Glu), but even as a stand-alone, it is involved in redox control and metabolic switches, promoting adenosine triphosphate (ATP) production as a donor for the electron transport chain (ETC) via hydrogen sulfide (H_2S) [9,10].

Sulfhydryl-rich molecules have been widely tested in the presence of oxidative stress as the modulation of redox-active thiols leads to the restoration of GSH levels and may activate the anti-oxidant signaling cascade [11]. ECs rely mainly on glycolysis rather than oxidative phosphorylation (OXPHOS) for energy production to keep ROS levels at a minimum [12,13]. Previous studies on ECs in hypoxic conditions highlighted the re-establishment of GSH levels and the amelioration of

* Corresponding author.
E-mail addresses: michela.bruschi@uniurb.it (M. Bruschi), s.masini3@campus.uniurb.it (S. Masini), federica.biancucci@uniurb.it (F. Biancucci), giovanni.piersanti@uniurb.it (G. Piersanti), barbara.canonico@uniurb.it (B. Canonico), michele.menotta@uniurb.it (M. Menotta), mauro.magnani@uniurb.it (M. Magnani), alessandra.fraternale@uniurb.it (A. Fraternale).

https://doi.org/10.1016/j.bbagen.2025.130803
Received 19 December 2024; Received in revised form 27 March 2025; Accepted 1 April 2025
Available online 3 April 2025

oxidative stress via a redox-modulating compound providing cysteines and sulfhydryl groups, i.e., I-152 [14]. This compound fuses *N*-acetylcysteine (NAC) and cysteamine (MEA), which are slowly released within the cells after the metabolic conversion [15]. Thanks to its acetyl group, I-152 can easily cross the phospholipidic membranes to be metabolized within the cell. The effects of I-152 have already been reported in murine *in vitro* and *in vivo* models, showing superior properties with respect to parental drugs, combined or singularly applied, in boosting GSH, activating Nrf2, [11] and modulating several redox-dependent functions, i.e., immune response [16,17]. Thus far, the investigation of I-152 on human ECs was performed to face a hypoxia-dependent GSH depletion [14]; however, the effects of the compound on the cell metabolism in physiological conditions is likewise important to obtain information about possible I-152-inducible reductive and/or oxidative stress. To further dissect the role of I-152 treatment on ECs, cells were pre-treated with the molecule before being co-cultured with lipopolysaccharide (LPS)-stimulated macrophages (THP-1). A thorough understanding of the metabolic changes of ECs upon redox-modulatory treatment is necessary for developing future therapeutics since targeting redox alterations in dysfunctional or diseased tissues may lead to metabolic perturbations in healthy cells.

Abbreviations: ADP adenosine diphosphate, AMP adenosine monophosphate, ATP adenosine triphosphate, Cys cysteine, ECs endothelial cells, FAS fatty acid synthase, GDH glutamate dehydrogenase, GSH reduced glutathione, GR glutathione reductase, GSSG oxidized glutathione, HK hexokinase, HO-1 heme-oxygenase 1, HSCs hematopoietic stem cells, HUVECs human umbilical endothelial cells, IDH isocitrate dehydrogenase, iNOS induced nitric oxide synthase, LFQ label-free quantification, LPS lipopolysaccharide, MDH malate dehydrogenase, MEA *S*-acetyl-β-mercaptoethylamine, NAC *N*-acetylcysteine, NACMEAA dithiol, NAD nicotinamide adenine dinucleotide, NADP nicotinamide-adenine-dinucleotide phosphate, OCR oxygen consumption rate, PGK phosphoglycerate kinase, ROS reactive oxygen species, SDH succinate dehydrogenase, SPDS spermidine synthase, TPI triosephosphate isomerase, VEGF vascular endothelial growth factor, WSP-5 washington state probe 5.

2. Materials and methods

2.1. I-152 synthesis

I-152 was synthesized following previously established protocols (compound 6 in Supplementary files page 11 [18]). The compound is constituted by a combination of *S*-acetyl-β-mercaptoethylamine (MEA) and *N*-acetyl-cysteine (NAC) linked together by an amide bond.

2.2. Cell culture

HUVECs (Lonza, Switzerland) were cultured in endothelial growth medium 2 (EGM-2™) supplemented with EGM-2 BulletKit™ (Lonza) and used between passages 4–7. I-152 at a concentration of 30 μM was added to the cell culture medium of 0.5×10^6 cells/well. Treated cells were kept in the incubator with 5 % CO_2 at 37 °C with a control group without the molecule.

2.3. Seahorse flux analysis

Assays were performed using an XFp Extracellular Flux Analyzer (Agilent, USA). HUVECs were seeded on Seahorse XFp mini-culture plates in XF Seahorse DMEM medium supplemented with 2 % FBS at 10×10^3/well. Cells were treated with I-152 (30 μM) for 6 h and 24 h before proceeding with the measurements ($n = 3$ biological replicates and 3 technical replicates/cartridge). According to the manufacturer's protocol, the cells' oxygen consumption rate (OCR) and the extracellular acidification rate (ECAR) were determined using the XF Real-time ATP rate assay kit to measure oxidative phosphorylation and glycolysis, respectively. Briefly, three basal OCR measurements were taken, followed by sequential injections of 1 μM oligomycin A, an inhibitor of the ATP synthase, and a mixture of 0.5 μM rotenone A and 0.5 μM antimycin A, inhibitors of the complexes I and III. Three measurements following each treatment were taken. Glyco-ATP and mito-ATP were derived from cells sequentially treated with oligomycin A and Rot/Antimycin A. Activity measurements for the ATP production rate in ECs were performed according to the company guidelines.

2.4. Mitochondrial ROS detection

After 6 h and 24 h treatment, cells ($n = 3$ biological replicates and 3 technical replicates) were detached using 10 % Trypsin and labeled with MitoSOX Red (PerCP-Cy5, 5 μM) (Invitrogen, USA) for 20 min at RT in the dark. Experiments were carried out with a FACS Canto II flow cytometer (BD, USA), and analyses were performed using FACS Diva™ software; ~15,000 cell events were acquired for each sample. Data were quantified as fold change of medium fluorescent intensity (MFI) compared with control.

2.5. Thiol detection in HPLC

HUVECs (0.5×10^6 cells/T25 flask) (n = 3 biological replicates) were treated with 30 μM I-152 in the culture medium for 6 h and 24 h before being lysed with 100 μL of lysis buffer (0.1 % Triton X-100, 0.1 M Na_2HPO_4, 5 mM EDTA, pH 7.5) followed by 15 μL of 0.1 N HCl and 140 μL of precipitating solution [100 mL containing 1.67 g (w/v) of glacial metaphosphoric acid, 0.2 g (w/v) of disodium EDTA and 30 g (w/v) of NaCl] for GSH, NAC, MEA and cysteine detection in HPLC. Lysed samples were kept in ice for 10 min and then centrifuged at 12,000*g* for 10 min at 4 °C before 25 % (v/v) Na_2HPO_4 0.3 M and 10 % (v/v) DTNB were added to the supernatant solution where thiols were determined through a BDS Hypersil™ C18 column (5 μm, 150 × 4.6 mm) (Thermo Scientific, USA). Separation and elution conditions were previously described elsewhere [11]. Following the detection at 330 nm, quantitative measurements were compared with known concentration standards and normalized on the protein content, which was determined via Bradford assay. Control groups did not receive the treatment with the compound.

2.6. Mass spectrometry analyses

HUVECs, treated or untreated with I-152, were seeded at 5×10^6 cells per T75 flask for each condition ($n = 3$ biological replicates and 3 technical replicates). After 6 h and 24 h, cells were washed with ice-cold PBS and harvested in cold 80/10/10 LC/MS grade methanol/acetonitrile/water (Carl Roth, Karlsruhe, Germany). Insoluble material was pelleted by centrifugation at 20,000 *g* for 20 min. Acidic extraction buffer containing 20 mM ammonium acetate and 2.0 mM Na-ascorbate in 100 % methanol was prepared following the protocol established by Petrova and colleagues [19] to preserve redox-sensitive metabolites in parallel to global metabolic profiling of mammalian cells.

Samples were analyzed via ultra-high-pressure liquid chromatography Vanquish system (Thermo Fisher Scientific, USA) coupled to mass spectrometry Exploris 240 (Thermo Fisher Scientific) following previously published instructions [14].

Compounds were separated by both C18 Hypersyl GOLD column (150 × 2.1 mm × 1.9 μm,) and by the amide- HILIC Column (150 × 2.1 mm 2.6 μm both from Thermo Fisher Scientific). Acquisitions were performed in positive and negative ion polarity modes. The Exploris 240 was set in the MS1 range of 80–900 m/z, and 120,000 resolution at m/z 200, AGC target $10e^6$, and auto maximum injection time. For MS2, auto m/z range, stepped HCD normalized collision energy (20, 50, 80, 150 %), and 30,000 resolution at m/z 200, AGC target 2e5 and maximum injection time 70 ms. Calibration was performed before each analysis sequence, and the internal calibrant was employed in run start mode.

The untargeted metabolomics was performed by using the deep scan AcquireX software, with 5 ID runs, 5 quality control, and 3 replicates of each sample for statistical analysis. Raw data were processed by Compound Discoverer software Ver 3.3 (Thermo Fisher Scientific). Metabolite variations were set with a linear fold change of 1.5 and FDR <0.05.

Protein pellets ($n = 3$ biological replicates and 3 technical replicates) were dissolved in the EasyPep lysis buffer (Thermo Fisher Scientific, USA) and 50 μg were subsequently processed by the EasyPep™ Mini MS Sample Kit (Thermo Fisher Scientific). Purified peptides were employed in label-free bottom-up proteomic analysis. Briefly, one μg of peptides from each experimental condition were injected into the UltiMate™ 3000 RSLC nano System coupled to an Orbitrap Exploris 240 Mass Spectrometer (Thermo Fisher Scientific, Germany). Peptides were inline desalted by Acclaim PepMap C18 trap Column (5 μm, 0.3 mm × 5 mm Thermo Scientific), and then resolved by Easy-Spray Pepmap RSLC C18 (2 μm, 75 μm × 50 cm) at a flow rate of 250 ml/min by a linear gradient of phase B (80 % acetonitrile/0.1 % formic acid, solvent A was 0.1 % formic acid in water) from 2 % to 50 % in 200 min, to 95 % in 20 min, kept for 10 min and then the column was re-equilibrated for 10 min. Data were acquired in a positive mode and in a data-dependent manner. For MS1 m/z range was set to 350–1500 at 120,000 resolution (at m/z 200), AGC target $3e^6$, and auto maximum injection time. For MS2, switch to DDA when ions intensity was above $5e^3$, with m/z range in auto mode. Top 20 strategy was adopted with a dynamic exclusion time of 80 s and 10 ppm tolerance. HCD normalized collision energy was set to 30 %, AGC target $7{,}5e^4$, and maximum injection time 40 ms. Resolution was set to 15,000 at m/z 200, and internal calibrant was employed in run start mode. Raw data were engaged in Proteome Discoverer software v2.5 (Thermo Fisher Scientific USA), adopting the label-free signal quantification strategy.

2.7. Time-dependent H_2S detection

H_2S detection was carried out using 5 mg of the fluorescent probe WSP-5 (Washington state probe 5) (Sigma Aldrich, Germany), diluted in 2 mL DMSO to achieve a 3 mM stock solution. HUVECs were seeded at 5×10^4/well in clear-bottom 96-well plates and treated for 2 h, 6 h, and 24 h with 30 μM I-152. At these time points, a final WSP-5 concentration of 100 μM for 200 μL cell medium volume was added to the wells. Upon transfer to a 96-well black plate, the fluorescence intensity was measured every minute for 30 min using a Multiskan FC plate reader (Thermo Scientific, USA) at 37 °C with $\lambda_{ex}/_{em} = 502/525$ nm as described in previously established protocols [20,21]. Sodium sulfide (Na_2S) (50 μM) was used as a positive control, whereas cell culture medium and medium supplemented with 30 μM I-152 were included as negative controls.

2.8. Co-culture with THP-1 macrophages

THP-1 monocyte cells (6×10^5/well) ($n = 3$ biological replicates) were seeded in the apical chamber of Transwell© inserts (0.4-μm pore size and 12 mm diameter) in 1 mL of RPMI medium (supplemented with 10 % FBS, 1 % L-glutamine, and 1 % penicillin-streptomycin) and allowed to differentiate for 72 h at 37 °C and 5 % CO_2 using 20 ng/mL PMA (Sigma Aldrich, Germany). After 72 h, cells were stimulated with 10 μg/mL lipopolysaccharide (LPS) for 4 h, and unstimulated THP-1 cells were used as controls. Media were removed from all macrophage wells and replaced with 1 mL of co-culture EGM-2 media. Transwell© inserts containing THP-1 were transferred to HUVEC-seeded wells (1×10^5 cells/well). An additional mL of co-culture media was added to the chambers. All samples were incubated for 24 h at 37 °C and 5 % CO_2. HUVEC cultured in the absence of macrophages served as controls. Controls were cultured in equal volumes of media to account for changes in cell behavior induced by media supplements.

After 24 h, Transwell© inserts were removed, and HUVECs were washed in 1× PBS to remove residual media. Cells were lysed directly either in 350 μL of RLT Buffer (Qiagen, USA) for RNA extraction or lysis buffer together with precipitating solution as described in section 2.5 for GSH and cysteine detection in HPLC.

2.9. Real-time PCR

HUVEC lysates were mixed with an equal volume of 70 % ethanol and directly loaded onto RNeasy mini-spin columns (RNeasy Micro Kit, Qiagen, USA) for purification, according to the manufacturer's instructions. RNA was eluted and quantified on a NanoDrop 1000 (Thermo Scientific, USA). Complementary DNA (cDNA) was synthesized from 250 ng of RNA (A260/280 > 1.8) using the PrimeScript RT-PCR Takara Kit (Takara Bio Inc., Japan). Quantitative reverse transcription PCR (RT-PCR) was performed using PowerUp™ SYBR Green Master Mix (Applied Biosystems) according to the manufacturer's instructions. The expression of target genes was normalized to the reference gene, β-actin (*β-ACT*). All primers were synthesized by Sigma Aldrich: Interleukin-8 (*IL-8*), 5′-TTGCCAAGGAGTGCTAAAGAA-3′ (forward) and 5′-GCCCTC TTCAAAAACTTCTCC-3′ (reverse); Vascular endothelial growth factor (*VEGF*), 5′-TCACAGGTACAGGGATGAGGACAC-3′ (forward) and 5′-CAAAGCACAGCAATGTCCTGAAG-3′ (reverse); *β-ACT*, 5′-ACCTAACTT GCGCAGAAAACA-3′ (forward) and 5′-AACAATGTGCAATCAAAGTCCT-3′ (reverse); Heme oxygenase-1 (*HO-1*) 5′-CCAGCAACAAAGTGCAA-GATTC-3′ (forward) and 5′-TCACATGGCATAAAGCCCTACAG-3′ (reverse); Inducible nitric synthetase (*iNOS*): 5′-GCTCTACACCTCC AATGTGACC-3′ (forward) and 5′-CTGCCGAGATTTGAGCCTCATG-3′ (reverse); Intercellular Adhesion Molecule 1 (*ICAM-1*): 5′-AGCGGCT-GACGTGTGCAGTAAT −3′ (forward) and 5′-TCTGAGACCTCTG GCTTCGTCA-3′ (reverse); Vascular cell adhesion protein 1 (*VCAM-1*): 5′-GATTCTGTGCCCACAGTAAGGC-3′ (forward) and 5′-TGGTCACA-GAGCCACCTTCTTG-3′ (reverse).

2.10. Glutathione reductase (GR) activity

GR enzyme (Sigma Aldrich, Germany) was incubated for 4 h with the same concentration of I-152, NAC, and NACMEAA (30 μM) separately at 37 °C in PBS solution. GR catalyzes the reduction of GSSG by NADPH to GSH. Therefore, GR activity was assayed directly following the protocol described by Ernest Beutler [22]. Briefly, the reagents for enzymatic activity were added to 79 μL H_2O volume as follows: 5 μL TRIS-HCl (1 M pH 8.0) with EDTA (5 mM), 1 μL of sample, 10 μL GSSG (20 mM in water), and 5 μL NADPH (2 mM). The activity of the enzyme was measured by following the oxidation of NADPH spectrophotometrically at 340 nm for 10 min after the start of the reaction using a Multiskan FC plate reader (Thermo Scientific, USA). The decrease in NADPH absorbance (ΔΔ) without GSSG was determined and subtracted from the corresponding assays, to give the net GR activity.

2.11. I-152 reducing capacity

The product of GSSG reduction, i.e., GSH, was evaluated after 1 h incubation at 37 °C of 25 μM GSSG with increasing concentrations of I-152 (10, 25, 50, 125, and 250 μM) in PBS solution. GSH content was determined by an HPLC method based on separation coupled with ultraviolet detection and pre-column derivatization with 5,5′-dithiobis-(2-nitrobenzoic acid) as described in section 2.8.

2.12. Statistical analyses

Data are represented as the mean ± SD, and *p*-values were determined by one-way or 2-way ANOVA with Tukey's post hoc test using Prism (GraphPad version 10.4.0). Significance is indicated with asterisks *, and a minimum *p*-value of 0.05 was considered statistically significant. For metabolomic analysis, ANOVA statistic was adopted, followed by the Tukey HSD test, a *p*-value of 0.05 was considered statistically significant. For proteomic data, the peptide identification adopted the

false discovery rate evaluation by a target-decoy strategy in a concatenated *q*-value manner. FDR (strict) was set as 0.01, while FDR (relaxed) was set as 0.05. Differentially expressed master proteins (log2 fold change 0.3 and $p < 0.05$) were selected and subsequently evaluated. Proteins upregulated by the compound (fold change >1.5) were analyzed via the STRING database (v.11.5) [23,24] for functional enrichment in biological processes (Gene Ontology), considering FDR < 0.003 and default parameters.

3. Results and discussion

Endothelial cells (ECs) line the inner surface of the vascular system. ECs have a glycolytic phenotype in physiological conditions, but they undergo metabolic changes upon *stimuli*, including hypoxia, inflammation, and immune stimulation [2,5,12].

The increased intracellular bioavailability of cysteine, thanks to I-152, is itself a *stimulus* for metabolic remodeling. Glycine, cysteine, and glutamate constitute GSH, which is essential for maintaining the redox state and allowing cellular metabolic functioning. Cysteine can supply all metabolic pathways that generate electron donors participating in oxidative phosphorylation; in fact, cysteine degradation releases H_2S, which is itself an electron donor for ETC [9]. Indeed, the enzyme sulfide: quinone oxidoreductase (SQR) can extract electrons from H_2S, delivering them into the quinone pool, thus permitting entry into the ETC at the level of complex III [25].

This study focused on some aspects of the metabolic state of ECs after 6 h and 24 h of I-152 treatment combined with the proteomic portrait at the latter time point, followed by the resultant effect of such profile towards pro-inflammatory signals.

3.1. ATP production rate in glycolysis and oxidative phosphorylation

The intracellular redox balance or redox status is a dynamic system that may change through many factors. Mitochondria are the primary intracellular energy source, generating ATP through the tricarboxylic acid cycle (TCA), and particularly, OXPHOS [26,27]. When facing physiologically hypoxic conditions, ECs rely mainly on glycolysis to produce ATP, avoiding the need for oxygen. Furthermore, the aerobic nature of cellular respiration makes ROS inevitable by-products of OXPHOS. Mitochondrial ETC is, in fact, the major contributor to ROS accumulation [28]. The influence of thiol-based redox modification on hypoxic ECs was previously described elsewhere, and the experimental concentration of I-152 (30 μM) was selected based on those results [14]. Nevertheless, the effects of the compound on ECs that are not subjected to hypoxia-dependent oxidative stress have been evaluated in this study. HUVECs were selected as a model for ECs, and mitochondrial respiration was investigated via seahorse ATP real-time assay (Fig. 1A), whereas mitochondrial stress upon treatment was evaluated in the form of ROS production via flow cytometry using MitoSOX™ labeling. The glycolytic ATP production rate did not show differences at both time points, while the mitochondrial ATP rate increased at both 6 h and 24 h with the I-152 treatment compared to the corresponding untreated groups. However, the stimulation of oxygen consumption in mitochondria (Fig. 1B) was not accompanied by an increase in ROS level (Fig. 1C), indicating that the physiological baseline of cellular ROS was preserved. This is a pivotal point since a moderate amount of ROS has been involved in a series of pleiotropic signals acting as a second messenger and modulating cytoskeleton dynamics as well as calcium release in physiological conditions [28–30].

3.2. Metabolomic and proteomic study

A non-targeted metabolomic approach was applied to deepen the links between changes in redox status and cell metabolism [31,32] as well as to identify the main metabolites that had undergone I-152 influence. This analysis allows the detection of a global metabolomic profile through HILIC and C18 columns in positive and negative acquisition mode, and, from ~20,000 metabolites, 1500 were identified and listed in Supplementary material S1. Firstly, intracellular I-152 metabolism was investigated. The chemical structures of I-152 and its metabolites were depicted in combination with the conceivable formation reactions (Fig. 2A). Mass spectrometry revealed I-152 itself and its derivatives, e.g., the triacetylated and NACMEAA forms, in addition to NAC, at both time points, confirming the ability of the compound to cross the cell membrane and be metabolized mainly within the cell (Fig. 2B). After deacetylation to the corresponding NACMEAA, NAC, and MEA are released [15]. MEA could be partially converted into cystamine upon oxidation of its sulfhydryl group and/or form a mixed disulfide [33] HPLC quantification of pivotal metabolites after 2 h, 6 h, and 24 h of treatment with respect to control (Fig. 2C) exhibited increasing

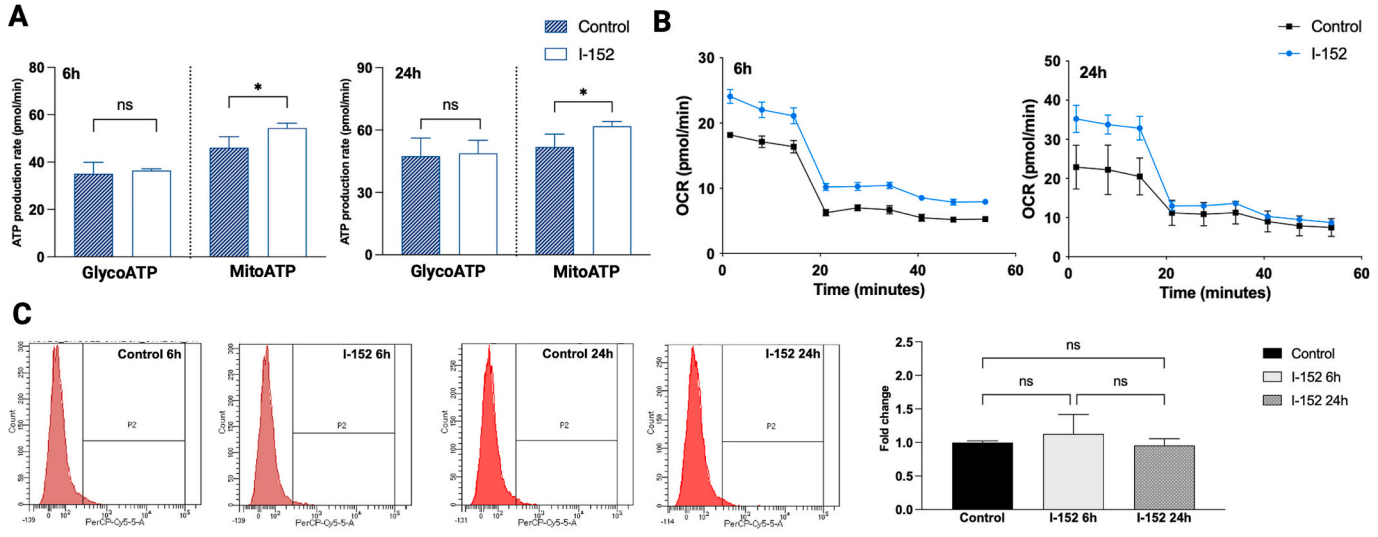

Fig. 1. (A) Metabolic flux analysis showing total quantification of mitochondrial ATP (Mito) and glycolytic ATP (Glyco) production rate via Seahorse XFp Real-Time. Separate glycolytic and mitochondrial ATP analyses were performed in HUVECs under control conditions or after 30 μM I-152 treatment for 6 h and 24 h. Statistical analysis was performed on the sum of glycol and mito ATP. (B) Kinetic profile of Seahorse OCR measurements following I-152 treatment at 6 h and 24 (C) Flow cytometry analysis of HUVECs treated for 6 h and 24 h with I-152 using MitoSOX (PerCP-Cy5) for mitochondrial ROS detection: representative histograms (left) and statistical analysis (right). Data were expressed as mean ± SD ($n = 3$ biological replicates and 3 technical replicates) * $p < 0.05$.

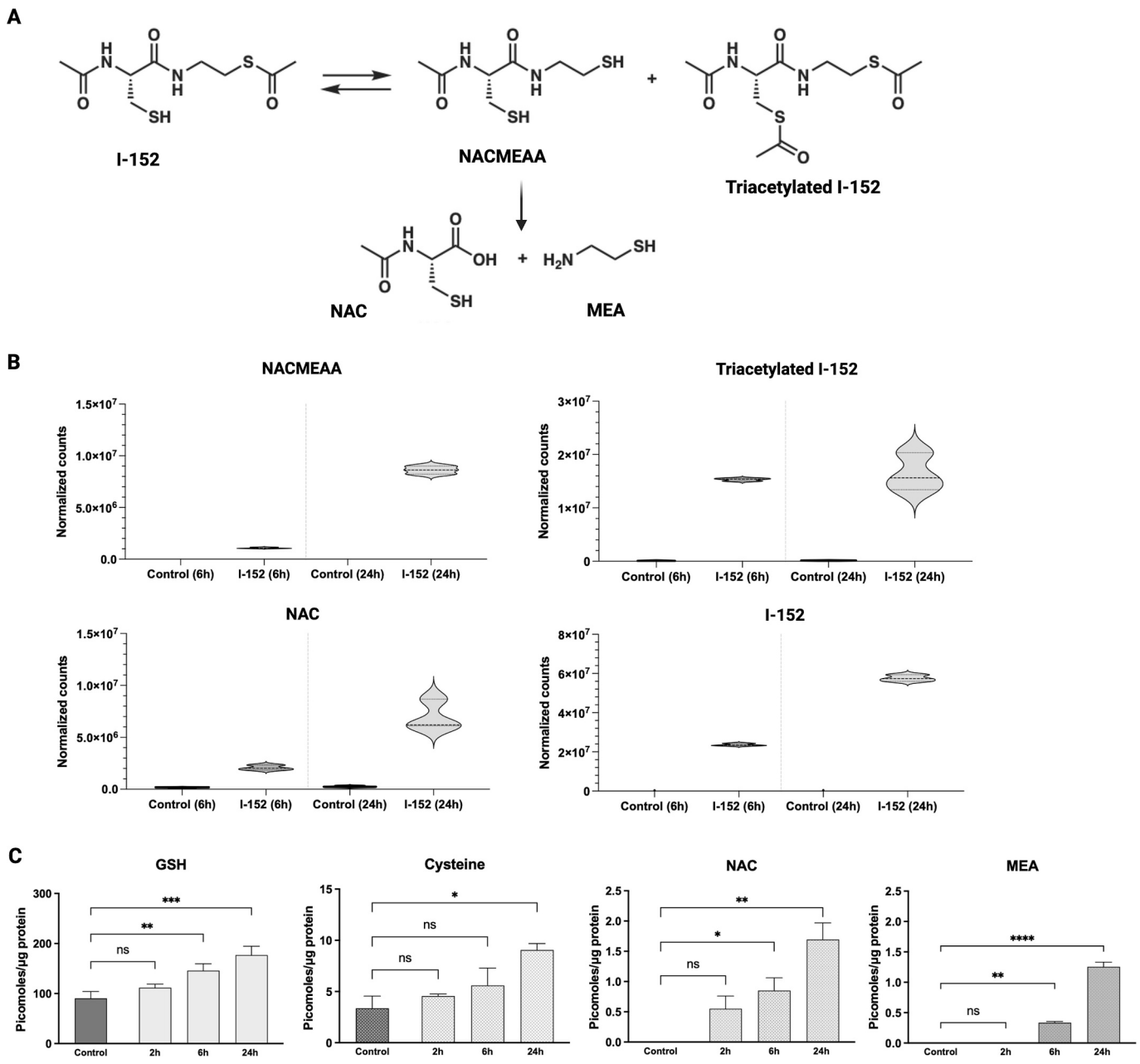

Fig. 2. (A) Chemical structure depiction of I-152 and its derivatives (NACMEAA, NAC, MEA, Triacetylated I-152) (B) The relative amount of I-152 and its metabolites (NACMEAA, Triacetylated I-152, and NAC) obtained via untargeted metabolomic analyses in HUVECs. ($n = 3$ biological replicates and 3 technical replicates) (C) GSH, cysteine, NAC, and MEA content (picomoles/µg protein) in HUVECs (n = 3 biological replicates) after 2 h, 6 h, and 24 h treatment with I-152 (30 µM) determined via HPLC analyses. Values represent the mean ± SD * $p < 0.05$, ** < 0.005, *** < 0.001, **** < 0.0001.

concentrations of GSH (up to 1.76-fold), cysteines (up to 2.83-fold), NAC (1.74 picomoles/ µg protein) and MEA (1.25 picomoles/ µg protein) while proceeding towards the latter time-point. The lower MEA content with respect to NAC, observed in HPLC, could reflect its partial oxidation, as mentioned above.

Further study of upregulated metabolites via enrichment pathways highlighted how GSH, purine as well as taurine metabolisms were among the routes positively modulated by I-152 at both 6 h and 24 h (Supplementary Material S2). To examine these routes in detail, a few metabolites have been selected for representation as a fold change versus their controls in violin plots (Fig. 3A); however, a full list of the up-downregulated metabolites from the metabolomic study is available in Supplementary Material S3, as a ratio between I-152-treated and untreated groups at 6 h and 24 h.

Furthermore, a proteomic study was performed at 24 h to complement the metabolic data. From the analyses using peptide and protein annotation nodes in Proteome Discoverer©, 10,069 peptide groups emerged, and among these, 3494 proteins (including isoforms) and 1017 master proteins were identified. The software considered the master protein to be the longest isoform of the identified proteins, tagging them as such through the applied nodes. The proteomic profiles of the two groups were displayed as a heatmap (Fig. 4A) showing the abundances of the identified proteins and depicting in white those that were absent in a specific group. The comparative study highlighted how from a total of 1017 master proteins, 684 were present in both groups, whereas 86 were expressed exclusively in control and 247 exclusively in the treated group (Fig. 4B). To understand which biological processes would be affected by these variations in the proteomic profile, a pathway

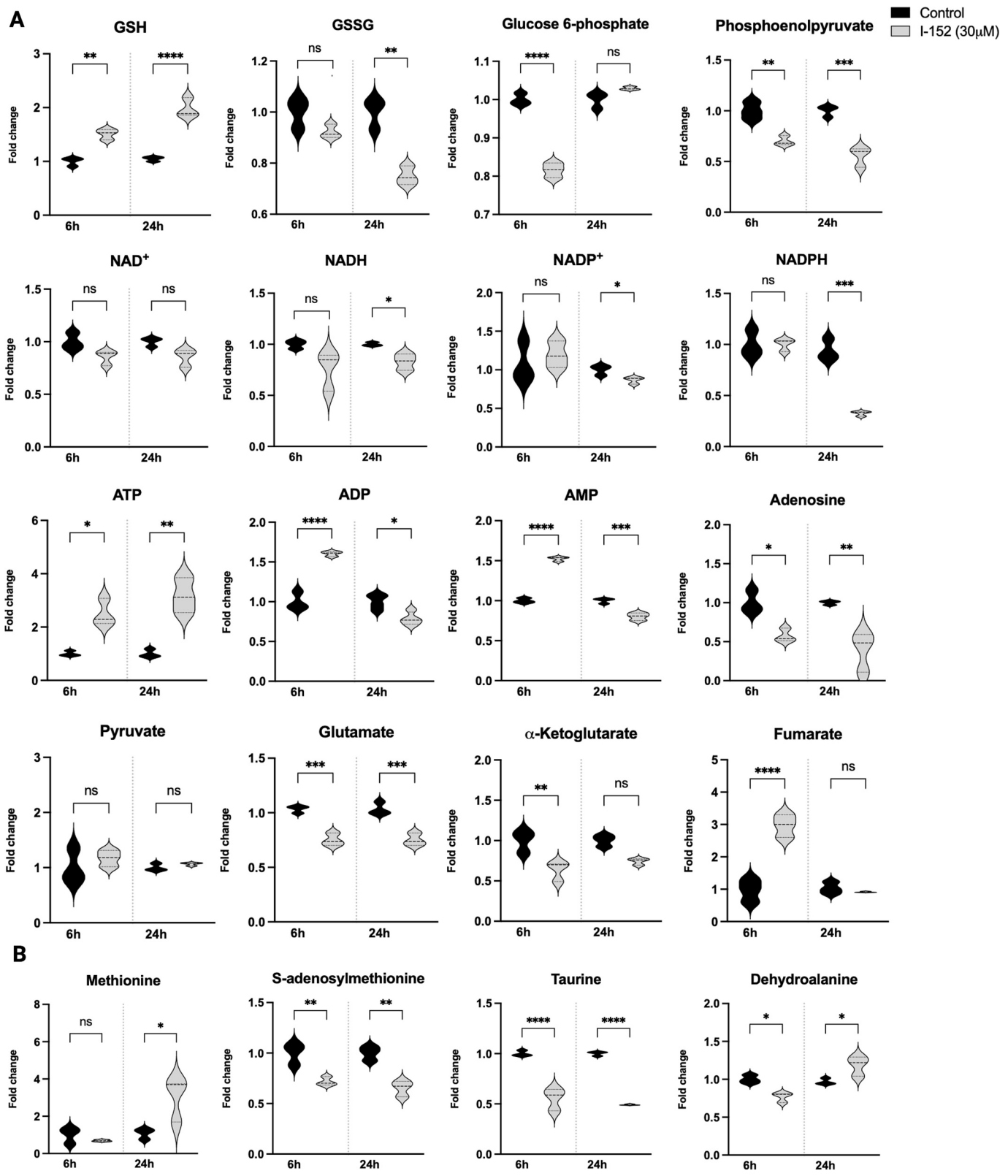

Fig. 3. (A) Highlights of some metabolites belonging to the redox system [GSH, GSSG, NAD(P)$^+$, NAD(*P*)H], glycolysis and penthose phosphate pathway [glucose 6-phosphate and phosphoenolpyruvate], TCA cycle [α-ketoglutarate, glutamate, fumarate and pyruvate], and nucleotide metabolism [ATP, ADP, AMP, Adenosine] in HUVECs treated with I-152 (30 μM) vs untreated control at 6 h and 24 h. (B) The transsulfuration pathway's main components [methionine, S-adenosylmethionine, taurine, and dehydroalanine]. Violin plotted values represent the fold change vs control ($n = 3$ biological replicates and 3 technical replicates). * $p < 0.05$, ** < 0.005, *** < 0.001, **** < 0.0001.

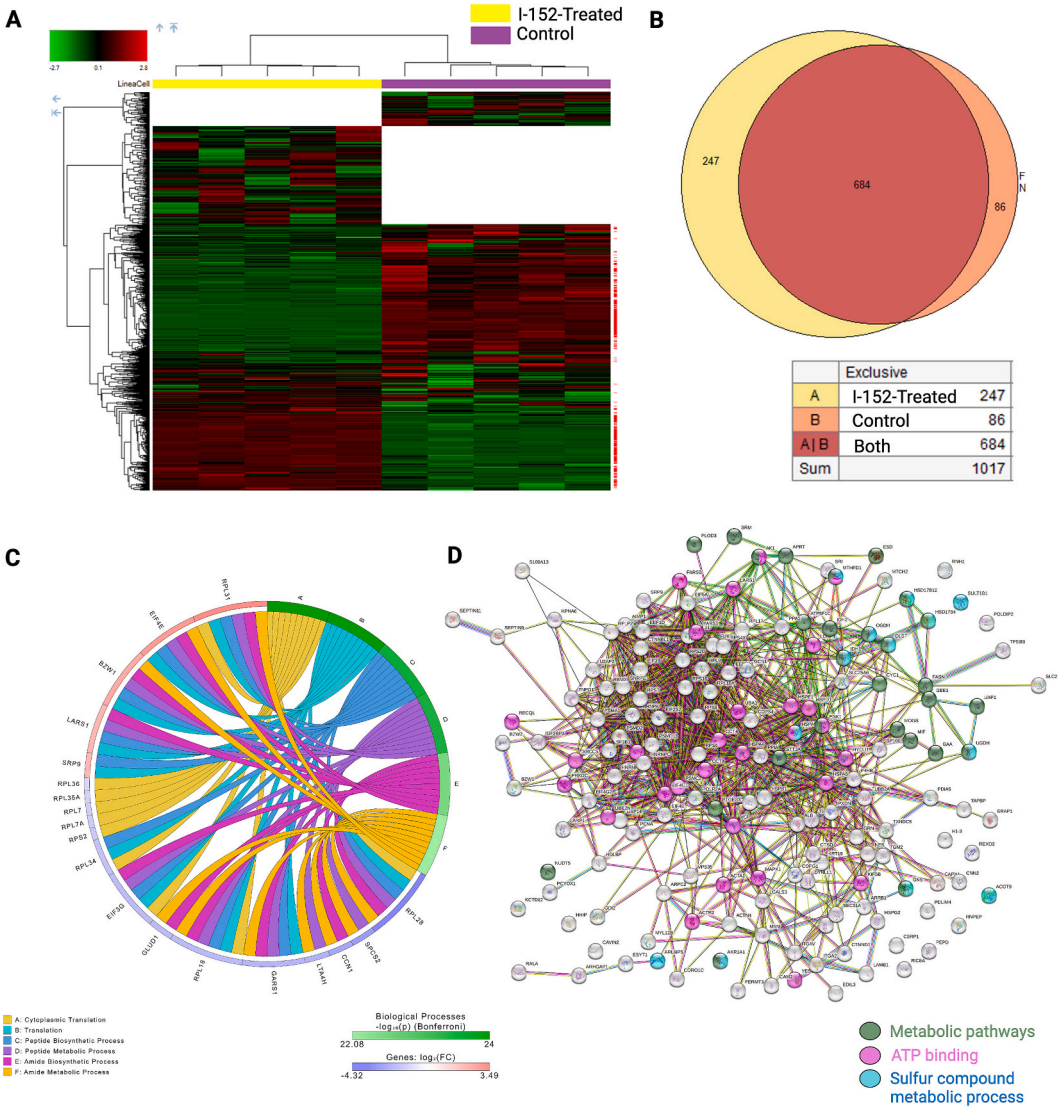

(caption on next page)

Fig. 4. (A) Heatmap displaying the proteomic profile of control and I-152-treated HUVECs for the identified 1017 proteins ($n = 3$ biological replicates and 3 technical replicates). The white color indicates the absence of proteins that were exclusively expressed by the counterpart. (B) Venn diagram of all 1070 identified master proteins, depicting that 684 were present in both groups, whereas 86 were expressed exclusively in control and 247 exclusively in the treated group. (C) Chord diagram from pathway analysis, obtained using iPathway Guide (Advaita Bio©) after Bonferroni corrections, showing the top six biological processes enriched with the treatment. Significant pathways are shown on the right, and the fold change of core genes is shown on the left. Left–right connections indicate the process membership in a pathway's leading-edge subset (D) STRING (v.11.5) network of significantly upregulated proteins upon I-152 treatment. Each node color represents a different pathway class that belongs to the metabolic pathways (green), ATP binding proteins (purple), and sulfur compound metabolic processes (blue). (E) Volcano plot showing proteome data and the mean difference of LFQ intensities between controls and I-152-treated cells versus statistical significance ($-\log_{10}$ of the *p*-value). The colored boxes show where the threshold was set by applying an FDR of 0.06. (For interpretation of the references to color in this figure legend, the reader is referred to the web version of this article.)

enrichment analysis was performed through the software iPathways Guide (Advaita Bio©) (Fig. 4C). From the enrichment, it emerged that amide biosynthetic and metabolic pathways were modulated by the treatment, but these results were not surprising, bearing I-152 and, specifically, its by-product NAC an amide group. A list of all the 346 modulated proteins is provided in Supplementary Material S4, presented as the fold change (whenever above 0.5) between I-152-treated vs untreated (I-152 treated vs untreated at 24 h) and the respective adjusted *p*-value. Further investigation of upregulated proteins (considering a $\log_2$ value of 0.6 statistically relevant) via the STRING database (Search Tool for the Retrieval of Interacting Genes/Proteins) [23,24] for functional enrichment in biological processes (Fig. 4D) highlighted how the majority of those proteins are involved in metabolic pathways (in green), ATP binding (in purple), and sulfur compound metabolic processes (in blue). Looking more in detail at the proteomic volcano plot (Fig. 4E), it is possible to highlight metabolic pathways whose enzymes participate in the glycolysis (i.e., hexokinase, phosphoglycerate kinase, and triosephosphate isomerase), Krebs cycle (i.e., malate, succinate, glutamate, isocitrate and 2-oxoglutarate dehydrogenases) and polyamine synthesis (spermidine synthase).

Mass spectrometry confirmed previous findings obtained via HPLC with respect to increased GSH levels with I-152 [14], and the decreased content of GSSG at 24 h prompted the idea of a reducing environment when the compound was applied (Fig. 3A). This condition could be correlated with the low levels of NADP/NADPH, which may be used as a reducing cofactor by the GR to salvage GSH from GSSG or as an electron source for the biosynthesis of fatty acids by an increased fatty acid synthase (FAS)(1.6 fold) as reported elsewhere [34,35]. Hence, increased GSH levels may be induced by I-152 through different mechanisms: 1) supplying amino acid precursors in the form of cysteine (as determined by HPLC), 2) activating the Nrf2 pathway [11], corroborated by a 6-fold increase in heme-oxygenase-1 (*HO-1*) mRNA transcription (Supplementary Material S5A), or 3) converting ~5 % of the GSSG into GSH thanks to the reducing capacity (Supplementary Material S5B). Nevertheless, the compound did not directly target GR enzymatic activity for the conversion GSSG-GSH (Supplementary Material S5C). These mechanisms could explain how such a small compound could influence the cellular energetic metabolism. Mitochondrial respiration and glycolysis are the major sources of adenosine triphosphate (ATP) for energy production, and higher ATP values were found via mass spectrometry in the treated group at both time points in parallel to a decrease in adenosine. The Seahorse data identified the modulation of ATP production from mitochondria, whereas ATP from glycolysis in both treated and untreated cells was not altered (Fig. 1A). On the other hand, as regards ADP and AMP, cells boosted these nucleotide productions at 6 h, declining then at 24 h to lean the ratio towards ATP (Fig. 3A). A reduction in NADH level at 24 h without fluctuation in NAD^+ content could indicate NADH consumption in the respiratory chain to sustain ATP synthesis. Therefore, besides affecting GSH, GSSG, and other members of the redox system, redox regulators may influence the energetic profile of ECs, eventually directing them to preferential OXPHOS for ATP production. As aforementioned, glycolic ATP did not show variations despite low glucose 6-phosphate level and downregulated hexokinase (HK), likely due to the upregulation of phosphoglycerate kinase (PGK) (2-fold) and increased dephosphorylation of phosphoenolpyruvate, leading to no statistical differences in pyruvate content (Fig. 3A). Less gluconate and low 6-phosphogluconolactonase (0.4-fold) could imply a minor input towards the pentose phosphate pathway, contributing to the low observed NADPH content. Indeed, the mass spectrometry analysis suggested that the observed metabolite fluctuations were the result of that specific moment and did seem to imply a faster or slower cycle performance in treated groups versus control. Even TCA was characterized at 6 h by a higher fumarate content, while there were no changes at 24 h. Instead, malate content was reduced at both time points, suggesting its usage in the cycle where key enzymes such as α-ketoglutarate dehydrogenase (OGDH) (also referred to as 2-oxoglutarate dehydrogenase) and isocitrate dehydrogenase (IDH) were upregulated (both ~2-fold). OGDH could interact with complex I of ETC, allowing a direct transfer of NADH to the NADH-oxidation site of Complex I, contributing to mitochondrial electron leakage [36], whereas IDH is known to play a pivotal role in energy homeostasis and to be controlled at the transcriptional level by Nrf2 [37]. Indeed, IDH deficiency could induce mitochondrial dysfunction, inhibit the activity of OXPHOS, and cause the production of ATP in the following step [38]. A metabolite linking energy and GSH metabolisms is glutamate, which was reduced in concomitance with the abated glutamate dehydrogenase (GHD) (0.18-fold). Glutamate, besides serving as a precursor for the α-ketoglutarate pool and the enhanced GSH synthesis, could also be converted through the urea cycle into ornithine, which increased together with *N*-acetylornithine and arginine at 24 h (Supplementary material S3). Arginine via ornithine could fuel the polyamine synthesis. In fact, ornithine was further metabolized to alkylamines such as polyamines, spermine, and spermidine [39], which were detected in high content as γ-Glutamyl-L-putrescine, N(1)-acetyl spermine, N(1), N(12)-diacetyl spermine sustained by enhanced spermidine synthase (6.1-fold) (Fig. 4B). Polyamines are essential for cell growth and proliferation; indeed, in ECs, proliferation is preceded by polyamine synthesis [40]. They could also prevent the decrease of intracellular GSH in case of stress via methionine mobilization and provide a cytoprotective effect [41]. Methionine itself, whose pathway, as mentioned, correlated with polyamines, was increased at 24 h in the presence of I-152, with a consequent reduction in S-adenosylhomocysteine, indicating that the cysteines required for GSH synthesis were provided by the compound and not necessarily derived from methionine through the transsulfuration pathway (Fig. 3B) thanks to the high amount of thiol species within the treated cells (Fig. 2B). We could also speculate that at 24 h, cysteines (together with glutamate) were mainly directed towards GSH formation and the release of H_2S as suggested by the concomitant increased dehydroalanine (Fig. 3B), a byproduct of spontaneous hydrogen sulfide loss from cysteines [42]. Concurrently, taurine synthesis was affected, resulting in low taurine levels (Fig. 3B). Indeed, cysteamine is also considered a precursor of taurine through the enzyme cysteamine dioxygenase, which converts it to hypotaurine by adding an oxygen molecule to the sulfhydryl group of cysteamine to produce hypotaurine [43]. Another mechanism could involve, in the presence of sulfur moieties, the formation of thiocysteamine, and Karpowicz and colleagues hypothesized that thiocysteamine spontaneously could subtract hypotaurine to generate thiotaurine by transferring its persulfide [44]. Both thiotaurine and hypotaurine would require hydrogen peroxide to be oxidized to taurine, and in our settings, this

process could be hindered. Nevertheless, these are hypotheses requiring further validation.

To recapitulate, the push in OXPHOS was conceivably linked to the release of H_2S (Fig. 5A) from cysteines (provided by the compound as is and in the form of NAC), which, besides supplying electrons for respiration, have been demonstrated to counteract ROS and increase the activity of antioxidant factors and pathways [45]. The H_2S production, revealed by the fluorescent probe WSP-5, was statistically prominent 2 h after 30 μM I-152 cell treatment. The fluorescent signal of I-152 in the medium (without cells) overlapped with that of the medium *per se* and could be considered negligible when compared to the response obtained with the cells. Thus, cells were essential for the metabolic conversion of the compound and H_2S release. The H_2S donor (Na_2S) was tested as WSP-5 positive control (Fig. 5B). Reports about H_2S turnover defined how its clearance could be monitored indirectly by oxygen consumption [46], which, indeed, increased dramatically with I-152 treatment (Fig. 1B). Moreover, H_2S could significantly increase Keap1 ubiquitination and decrease its combination with the transcription factor Nrf2 via Keap1 sulfhydrylation at Cys 151, 226, or 613 [47,48]. Indeed, Nrf2 has been shown to regulate different metabolic pathways and aspects of mitochondrial function, in particular, by increasing the efficiency of ATP production by OXPHOS [49]. The ability of I-152 to promote Nrf2 in a concentration-dependent manner was already demonstrated in another cell model [11]; however, Nrf2 activation in HUVECs was corroborated by *HO-1* mRNA expression at 24 h, which resulted in a 6-fold upregulation in the treated group (Supplementary Figure S5A). The next step was aimed to determine the possible outcomes of the new EC metabolic asset, i.e., boosted OXPHOS and GSH, towards a pro-inflammatory *stimulus* that would mimic the cell micro-environment in physiological conditions.

3.3. HUVECs-THP-1 co-culture

In previous studies, we demonstrated how I-152 could protect ECs against a direct insult, such as hypoxia [14]. In the current work, we investigated what could be the impact of redox modulation via the compound towards an indirect *stimulus*, such as the cellular crosstalk perturbed by inflammatory signals. For this aim, two pivotal members of the vascular and immune systems were chosen for co-culture: ECs and macrophages. THP-1 is a human monocytic cell line derived from an acute monocytic leukemia patient, and these cells have the potential to differentiate into macrophages through PMA, making THP-1 a valuable tool for investigating human macrophages in both health and disease. THP-1-derived macrophages were stimulated with 10 μg/mL LPS for 4 h, and after three washing steps, they were set in co-culture with HUVECs in a fresh medium. HUVECs were pre-treated or not with 30 μM I-152 for 2 h before the co-culture, and I-152 was removed before THP-1 addition to the top of the Transwell. With these settings, neither HUVECs had any direct contact with LPS nor THP-1 with I-152. LPS is a component of gram-negative bacteria, and it can be recognized by toll-like receptor-4 present on the macrophage surface. This co-culture system aimed to dissect the influence of EC new metabolic asset on the crosstalk between endothelial and macrophage cells.

At first, the addition of THP-1 to ECs caused a reduction in GSH levels and mobilization of cysteines in ECs (HUVECs/ THP-1 Control), further exacerbated when THP-1 cells were priorly stimulated with LPS (HUVECs/ THP-1 + LPS) (Fig. 6A) suggesting a redox perturbation, similar to that previously observed with a direct hypoxic *stimulus* [14]. These findings suggested that EC GSH is a redox-related biomarker of cellular stress induced by different inputs and that thiol molecules could be tools to restore redox balance. Indeed, the I-152 pre-treatment of ECs (HUVECs + I-152/ THP-1 + LPS) helped the intracellular redox sustainment, providing intermediate GSH values between the control and the pro-inflammatory stimulated group influencing interconnected pathways (Fig. 6A). Although crosstalk mechanisms are still poorly understood, inflammatory mediators are thought to play pivotal roles in angiogenesis.

ICAM-1 is an adhesion molecule constitutively present in ECs but can be induced by various inflammatory *stimuli*, and it is implicated in the development of vascular disease [50]. Kevil and colleagues demonstrated how high ICAM-1 interplays with intracellular GSH by hindering the glutamate-cysteine ligase and, as a consequence, its synthesis [51]. Like ICAM-1, VCAM-1 is an adhesion molecule supporting the adhesion of leukocytes to ECs. Besides their role in the recruitment, the inflammatory cytokines released by activated macrophages stimulate the expression of ICAM-1 and VCAM-1 by ECs [52]. Here, we have shown that I-152 down-regulated *ICAM-1* and *VCAM-1* mRNA expression in ECs within the inflammatory microenvironment (Fig. 6B). Proangiogenic signals have been linked to the activation of VEGF, a major inducer of vasculogenesis and neoangiogenesis in both physical and pathological conditions in a ROS-dependent mechanism [53]. VEGF induces an increase in intracellular ROS through the enhancement of mitochondrial metabolism, and in parallel, ROS stimulates VEGF expression [54,55]. *VEGF* expression at the transcriptional level was not affected in our system, but this could be due to a temporal delayed activation, as seen previously in the hypoxic model [14]. The inducible nitric oxide synthase (iNOS) expression has been associated with inflammatory areas in which macrophages and endothelial cells are distributed and where new vessel formation is promoted [56]. Hence, iNOS expression in ECs can occur following induction by LPS or inflammatory cytokines and generate large quantities of NO, resulting in EC activation and dysfunction [57]. Under our conditions, THP-1 cytokine production resulted in upregulated *iNOS* expression, whereas EC pretreatment with I-152 significantly reduced stress response (Fig. 6B). Another mediator of angiogenesis is interleukin-8, which promotes cell proliferation and survival [58]. It is mainly secreted from leukocytes and endothelial cells under exposure to pro-inflammatory *stimuli*. Previous studies using NAC demonstrated its inhibitory activity on both *ICAM-1* and *IL-8* when applied at a concentration of 30 mM (1000× higher than I-152) [59,60]; in our settings, I-152 lowered *IL-8* mRNA expression, although not

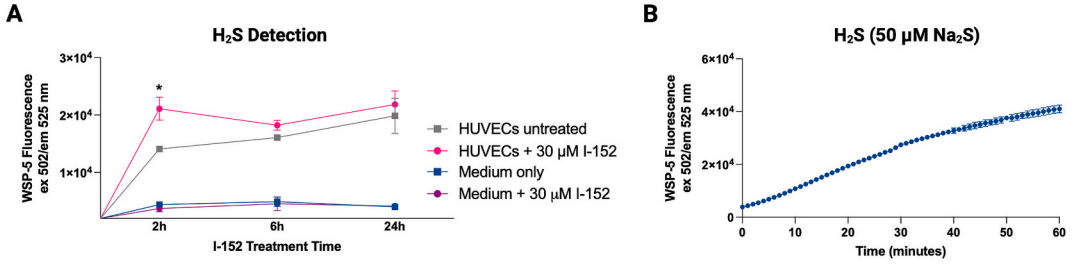

Fig. 5. (A) WSP-5 fluorescence response in HUVECs that were pretreated for 2 h, 6 h, and 24 h with 30 μm I-152 before adding 100 μM WSP-5 for 30 mins. The increase in fluorescence intensity was recorded in a black well plate at 37 °C using a microplate reader with λ ex/em = 502/525 nm and compared to untreated cells at the same time points. Cell medium alone and medium supplemented with 30 μm I-152 were used as negative controls. Results represent three different experiments, and data were expressed as mean ± SD, * p-value <0.05. (B) Time-dependent WSP-5 fluorescence response when HUVECs were exposed to 50 μM of Na_2S as H_2S donor for 60 mins (positive control). Plotted values are the mean ± SD of three experiments.

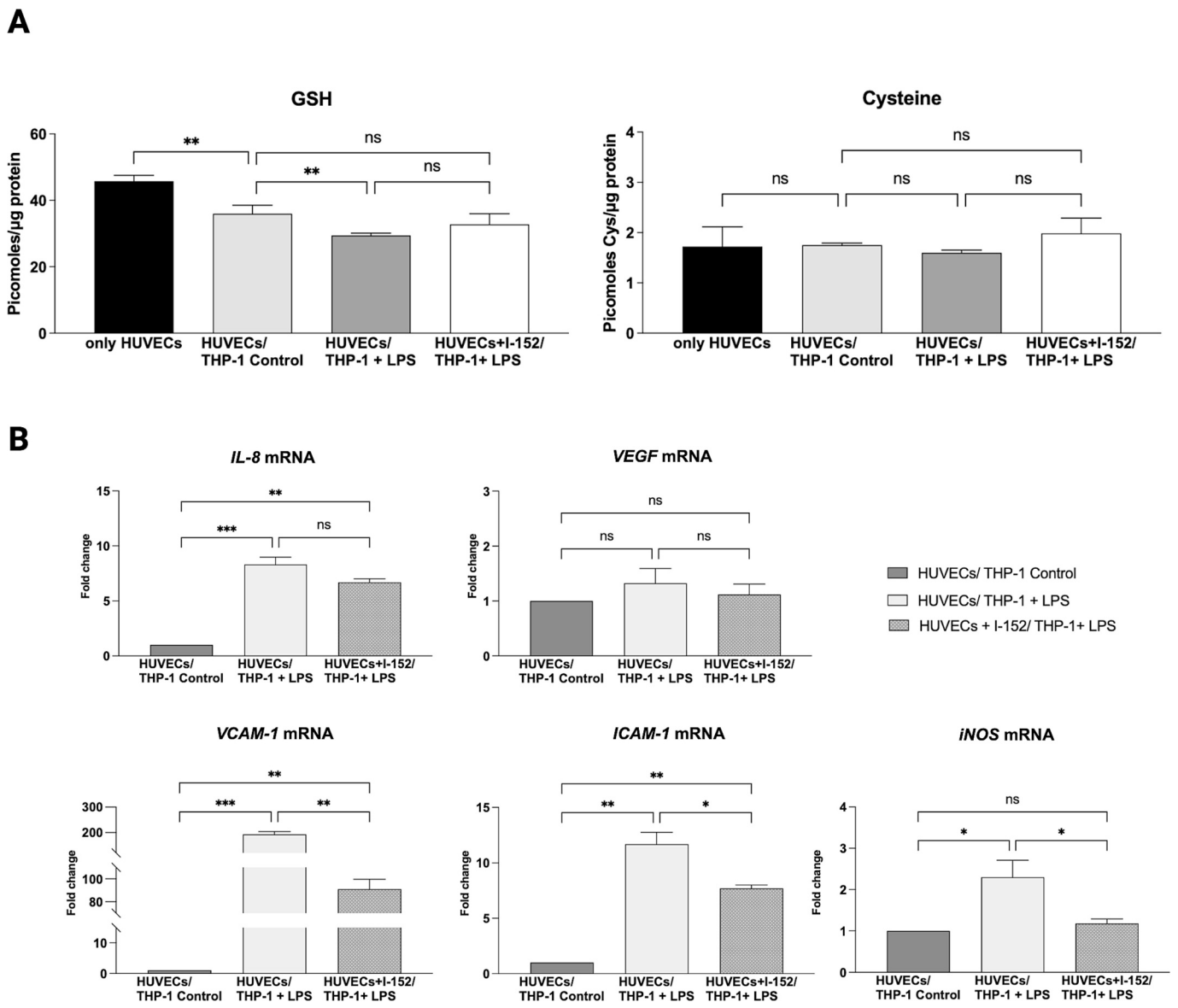

Fig. 6. (A) GSH and cysteine detection via HPLC in HUVECs co-cultured or not with THP-1 macrophages for 24 h. Four experimental groups were involved: 1) only HUVECs, comprehending cells alone without THP-1; 2) untreated HUVECs co-cultured with unstimulated THP-1 (HUVECs/THP-1); 3) HUVECs together with THP-1, that before being set in the co-culture received 10 µg/mL LPS for 4 h (HUVECs/THP-1 + LPS); 4) HUVECs treated with 30 µM I-152 for 2 h before co-culture with THP-1 previously stimulated with LPS (HUVECs +I-152 /THP-1 + LPS) (B) Relative expression of mRNA encoding *IL-8*, *VEGF*, *VCAM-1*, *ICAM-1* and *iNOS* on HUVECs calculated with the ΔΔ-Ct method using β-actin as a reference gene compared to controls. Three experimental groups were compared: HUVECs/THP-1 control, HUVECs/THP-1 + LPS, and HUVECs + I-152/THP-1 + LPS, following the above settings. Values are means from three different experiments ± SD. * $p < 0.05$, ** < 0.01 *** < 0.001.

statistically.

Overall, these results suggest that in the presence of O_2, the compound changed the metabolic profile towards mitochondrial respiration, fueling ATP production via OXPHOS without the downside of ROS generation, which could lead to endothelial dysfunctions [61]. The exact mechanism/s by which I-152 can modulate ROS overproduction has not yet been established. So far, the I-152 capacity of ROS scavenging has been ascribed to its GSH-boosting ability. However, I-152 provides a high amount of cysteine, and presumably consequent H_2S, that recent studies have demonstrated to inhibit *in vitro* and *in vivo* vascular inflammation, partly by ROS scavenging and partly by decreasing leukocyte adhesion via ICAM and VCAM downregulation [62,63]. An increased number of studies have confirmed the beneficial use of H_2S donors in oxidative stress-dependent diseases, ameliorating oxidative stress and inflammation [64]. Even though the role of H_2S in modulating redox signaling has still not been fully understood, H_2S could explicate their signaling effect through multiple mechanisms and interactions with different targets. In recent years, there has been increasing recognition of the importance of mitochondria in vascular endothelium damage, contributing to early events in atherosclerosis, hypertension, and diabetes. Endothelial dysfunction has been identified as a major mediator of cardiovascular diseases and is closely related to mitochondrial abnormalities that regulate the structure and function of endothelial cells themselves [65,66]. For these reasons, strategies employing redox-modulating compounds could become innovative drug candidates for disease prevention and treatment of ECs. Hence, applying I-152 as a redox modulatory agent in case of a localized disease could induce beneficial consequences without compromising the neighboring cells unaffected by oxidative stress. Nevertheless, further investigations encompassing *in vivo* models are necessary to fully understand the

potential effects of the compound on the cardiovascular system in terms of a systemic approach.

4. Conclusion

This study addressed how cellular energy metabolism was affected by fine-tuning the redox balance using thiols. Although antioxidants have been widely studied for their beneficial effects across multiple clinical indications, little information is available about redox modulation of cells in physiological conditions. I-152 demonstrated its activity in many oxidative settings, i.e., viral infections, hypoxia, etc., and is now complemented by this investigation on steady-state cells. The compound increased GSH content, providing precursors for its synthesis, such as NAC and cysteines, and sustained mitochondrial ATP production through the release of sulfhydryl groups and Nrf2 activation. Concurrently, the additional ROS derived from intensified OXPHOS electron leakage were presumably abated. The compound exhibited protective effects in ECs exposed to detrimental pro-inflammatory *stimuli* by hindering the expression of adhesion molecules and nitric oxide yield. Therefore, the I-152 application proved to be useful in pathological conditions, ameliorating stress-dependent parameters and, in steady-state cells, exerting a specific action on respiration and redox-related mechanisms without compromising cell functionality. Sulfur compounds, like I-152, could represent a useful pharmacological tool to be used in therapy or provide a template for designing new molecules with improved pharmacodynamics and pharmacokinetics. Further studies in animal models could offer the advantage of dissecting the systemic effect of the molecule and its metabolites beyond the pathological site or tissue as a potential therapeutic approach for diseases due to altered redox cellular balance.

Fundings

This work was supported by PRIN (Bando 2017; Prot. 2017Z5LR5Z to MMa) and the European Union fundings: - NextGeneration EU under the Italian Ministry of University and Research (MUR) National Innovation Ecosystem grant ECS00000041 - VITALITY - CUP H33C2200043000 to GP, BC, MMe and AF.

CRediT authorship contribution statement

Michela Bruschi: Writing – original draft, Validation, Software, Investigation, Formal analysis, Data curation. **Sofia Masini:** Validation, Data curation. **Federica Biancucci:** Validation, Methodology, Formal analysis. **Giovanni Piersanti:** Writing – review & editing, Resources, Funding acquisition. **Barbara Canonico:** Writing – review & editing, Methodology, Formal analysis, Data curation. **Michele Menotta:** Writing – review & editing, Software, Methodology, Formal analysis, Data curation. **Mauro Magnani:** Writing – review & editing, Supervision, Project administration, Funding acquisition. **Alessandra Fraternale:** Writing – review & editing, Supervision, Resources, Project administration, Funding acquisition.

Declaration of competing interest

The authors declare that they have no known competing financial interests or personal relationships that could have appeared to influence the work reported in this paper.

Data availability

Data will be made available on request.

Acknowledgments

The graphical abstract and Fig. 4 were created using BioRender.com. The access to BioRender.com was supported by Dr. Juho Parviainen (Palo Alto Networks, Inc.). Furthermore, we would like to thank POR MARCHE FESR 2014/2020. Asse 1, OS 2, Azione 2.1 - Intervento 2.1.1 – Sostegno allo sviluppo di una piattaforma di ricerca collaborativa negli ambiti della specializzazione intelligente. Thematic Area: “Medicina personalizzata, farmaci e nuovi approcci terapeutici”. Project acronym: Marche BioBank www.marchebiobank.it. «The content of the paper is the sole responsibility of the authors and can under no circumstances be regarded as reflecting the position of the European Union and/or Marche Region authorities».

Appendix A. Supplementary data

Supplementary data to this article can be found online at https://doi.org/10.1016/j.bbagen.2025.130803.

References

[1] M.D. Lee, et al., Small-world connectivity dictates collective endothelial cell signaling, Proc. Natl. Acad. Sci. U. S. A. 119 (2022) e2118927119.
[2] X. Li, X. Sun, P. Carmeliet, Hallmarks of endothelial cell metabolism in health and disease, Cell Metab. 30 (2019) 414–433.
[3] A. Antonelli, et al., Anoxia rapidly induces changes in expression of a large and diverse set of genes in endothelial cells, Int. J. Mol. Sci. 24 (2023) 5157.
[4] M. Bruschi, et al., Functionalized 3D scaffolds for engineering the hematopoietic niche, Front. Bioeng. Biotechnol. 10 (2022).
[5] G. Eelen, et al., Endothelial cell metabolism, Physiol. Rev. 98 (2018) 3–58.
[6] D. Nguyen, J.W. Hsu, F. Jahoor, R.V. Sekhar, Effect of increasing glutathione with cysteine and Glycine supplementation on mitochondrial fuel oxidation, insulin sensitivity, and body composition in older HIV-infected patients, J. Clin. Endocrinol. Metab. 99 (2014) 169–177.
[7] R. Parsanathan, S.K. Jain, Glutathione deficiency alters the vitamin D-metabolizing enzymes CYP27B1 and CYP24A1 in human renal proximal tubule epithelial cells and kidney of HFD-fed mice, Free Radic. Biol. Med. 131 (2019) 376–381.
[8] D. Alkazemi, A. Rahman, B. Habra, Alterations in glutathione redox homeostasis among adolescents with obesity and anemia, Sci. Rep. 11 (2021) 3034.
[9] J. Serpa, Cysteine as a carbon source, a hot spot in Cancer cells survival, Front. Oncol. 10 (2020).
[10] A. Lermant, C.E. Murdoch, Cysteine Glutathionylation acts as a redox switch in endothelial cells, Antioxidants 8 (2019) 315.
[11] R. Crinelli, et al., Activation of NRF2 and ATF4 signaling by the pro-glutathione molecule I-152, a co-drug of N-acetyl-cysteine and cysteamine, Antioxidants (Basel) 10 (2021) 175.
[12] B. Yetkin-Arik, et al., Endothelial tip cells in vitro are less glycolytic and have a more flexible response to metabolic stress than non-tip cells, Sci. Rep. 9 (2019) 10414.
[13] U. Topf, et al., Quantitative proteomics identifies redox switches for global translation modulation by mitochondrially produced reactive oxygen species, Nat. Commun. 9 (2018) 324.
[14] M. Bruschi, et al., The influence of redox modulation on hypoxic endothelial cell metabolic and proteomic profiles through a small thiol-based compound tuning glutathione and thioredoxin systems, Biofactors 49 (2023) 1205–1222.
[15] R. Crinelli, et al., Boosting GSH using the co-drug approach: I-152, a conjugate of N-acetyl-cysteine and β-mercaptoethylamine, Nutrients 11 (2019) 1291.
[16] A. Fraternale, et al., Targeting SARS-CoV-2 by synthetic dual-acting thiol compounds that inhibit spike/ACE2 interaction and viral protein production, FASEB J. 37 (2023) e22741.
[17] A. Fraternale, et al., Inhibition of myeloid-derived suppressor cell (MDSC) activity by redox-modulating agents restores T and B cell proliferative responses in murine AIDS, Int. Immunopharmacol. 124 (2023) 110882.
[18] F. Bartoccini, et al., Dithiol based on l-cysteine and Cysteamine as a disulfide-reducing agent, J. Org. Chem. 87 (2022) 10073–10079.
[19] B. Petrova, et al., Redox metabolism measurement in mammalian cells and tissues by LC-MS, Metabolites 11 (2021) 313.
[20] Y. Zhou, F. Mazur, K. Liang, R. Chandrawati, Sensitivity and selectivity analysis of fluorescent probes for hydrogen sulfide detection, Chem. Asian J. 17 (2022) e202101399.
[21] J.Lj. Miljkovic, et al., Rapid and selective generation of H2S within mitochondria protects against cardiac ischemia-reperfusion injury, Redox Biol. 55 (2022) 102429.
[22] E. Beutler, Glutahtione Reductase (GR), in: Red Cell Metabolism. A Manual of Biochemical Method 72–73, Grune & Stratton, Inc., 1984.
[23] L.J. Jensen, et al., STRING 8–a global view on proteins and their functional interactions in 630 organisms, Nucleic Acids Res. 37 (2009) D412–D416.

[24] D. Szklarczyk, et al., The STRING database in 2021: customizable protein-protein networks, and functional characterization of user-uploaded gene/measurement sets, Nucleic Acids Res. 49 (2021) D605–D612.
[25] B. Pedre, U. Barayeu, D. Ezeriņa, T.P. Dick, The mechanism of action of N-acetylcysteine (NAC): the emerging role of H2S and sulfane sulfur species, Pharmacol. Ther. 228 (2021) 107916.
[26] E. Georgieva, et al., Mitochondrial dysfunction and redox imbalance as a diagnostic marker of "free radical diseases", Anticancer Res. 37 (2017) 5373–5381.
[27] B.J.-A. Foo, J.Q. Eu, J.L. Hirpara, S. Pervaiz, Interplay between mitochondrial metabolism and cellular redox state dictates Cancer cell survival, Oxid. Med. Cell. Longev. 2021 (2021) e1341604.
[28] R.-Z. Zhao, S. Jiang, L. Zhang, Z.-B. Yu, Mitochondrial electron transport chain, ROS generation and uncoupling (review), Int. J. Mol. Med. 44 (2019) 3.
[29] L.S. Nakao, M.F. Olson, J.P. Vázquez-Medina, A. Valdivia, Editorial: reactive oxygen species (ROS) signaling during cytoskeleton dynamics, Front. Cell Develop. Biol. 11 (2023) 1295263.
[30] S. Negri, P. Faris, F. Moccia, Reactive oxygen species and endothelial Ca2+ signaling: brothers in arms or Partners in Crime? Int. J. Mol. Sci. 22 (2021) 9821.
[31] B. Ozyel, G. Le Gall, P.W. Needs, P.A. Kroon, Anti-inflammatory effects of quercetin on high-glucose and pro-inflammatory cytokine challenged vascular endothelial cell metabolism, Mol. Nutr. Food Res. 65 (2021) 2000777.
[32] E.B. Cohen, R.C. Geck, A. Toker, Metabolic pathway alterations in microvascular endothelial cells in response to hypoxia, PloS One 15 (2020) e0232072.
[33] C. Atallah, C. Charcosset, H. Greige-Gerges, Challenges for cysteamine stabilization, quantification, and biological effects improvement, J. Pharmaceut. Anal. 10 (2020) 499–516.
[34] W. Xiao, J. Loscalzo, Metabolic responses to reductive stress, Antioxid. Redox Signal. 32 (2020) 1330–1347.
[35] W. Xiao, R.-S. Wang, D.E. Handy, J. Loscalzo, NAD(H) and NADP(H) redox couples and cellular energy metabolism, Antioxid. Redox Signal. 28 (2018) 251–272.
[36] N. Kuksal, J. Chalker, R.J. Mailloux, Progress in understanding the molecular oxygen paradox – function of mitochondrial reactive oxygen species in cell signaling, Biol. Chem. 398 (2017) 1209–1227.
[37] C. Tonelli, I.I.C. Chio, D.A. Tuveson, Transcriptional regulation by Nrf2, Antioxid. Redox Signal. 29 (2018) 1727–1745.
[38] J.-B. Park, et al., IDH2 deficiency impairs mitochondrial function in endothelial cells and endothelium-dependent vasomotor function, Free Radical Biol. Med. 94 (2016) 36–46.
[39] M. Xuan, et al., Polyamines: their significance for maintaining health and contributing to diseases, Cell Commun. Signal 21 (2023) 348.
[40] W. Durante, Role of arginase in vessel wall remodeling, Front. Immunol. 4 (2013) 111.
[41] C. Wu, D.O. Kennedy, Y. Yano, S. Otani, I. Matsui-Yuasa, Thiols and polyamines in the cytoprotective effect of taurine on carbon tetrachloride-induced hepatotoxicity, J. Biochem. Mol. Toxicol. 13 (1999) 71–76.
[42] D. Benchoam, E. Cuevasanta, M.N. Möller, B. Alvarez, Hydrogen sulfide and Persulfides oxidation by biologically relevant oxidizing species, Antioxidants (Basel) 8 (2019) 48.
[43] J.E. Dominy, et al., Discovery and characterization of a second mammalian thiol dioxygenase, cysteamine dioxygenase, J. Biol. Chem. 282 (2007) 25189–25198.
[44] S.J. Karpowicz, L. Anderson, Enzymatic and non-enzymatic conversion of cystamine to thiotaurine and taurine, Biochim. Biophys. Acta Gen. Subj. 1866 (2022) 130225.
[45] V. Citi, et al., Role of hydrogen sulfide in endothelial dysfunction: pathophysiology and therapeutic approaches, J. Adv. Res. 27 (2021) 99–113.
[46] V. Vitvitsky, O. Kabil, R. Banerjee, High turnover rates for hydrogen sulfide allow for rapid regulation of its tissue concentrations, Antioxid. Redox Signal. 17 (2012) 22–31.
[47] M. Wang, et al., Exogenous H2S initiating Nrf2/GPx4/GSH pathway through promoting Syvn1-Keap1 interaction in diabetic hearts, Cell Death Discov. 9 (2023) 394.
[48] L. Xie, et al., Hydrogen sulfide induces Keap1 S-sulfhydration and suppresses diabetes-accelerated atherosclerosis via Nrf2 activation, Diabetes 65 (2016) 3171–3184.
[49] N. Esteras, A.Y. Abramov, Nrf2 as a regulator of mitochondrial function: energy metabolism and beyond, Free Radic. Biol. Med. 189 (2022) 136–153.
[50] W. Langston, et al., Regulation of endothelial glutathione by ICAM-1 governs VEGF-A-mediated eNOS activity and angiogenesis, Free Radic. Biol. Med. 42 (2007) 720–729.
[51] C.G. Kevil, et al., Regulation of endothelial glutathione by ICAM-1: implications for inflammation, FASEB J. 18 (2004) 1321–1323.
[52] P. d'Alessio, M. Moutet, E. Coudrier, S. Darquenne, J. Chaudiere, ICAM-1 and VCAM-1 expression induced by TNF-alpha are inhibited by a glutathione peroxidase mimic, Free Radic. Biol. Med. 24 (1998) 979–987.
[53] R. Colavitti, et al., Reactive oxygen species as downstream mediators of Angiogenic signaling by vascular endothelial growth factor Receptor-2/KDR*, J. Biol. Chem. 277 (2002) 3101–3108.
[54] M. Ushio-Fukai, R.W. Alexander, Reactive oxygen species as mediators of angiogenesis signaling: role of NAD(P)H oxidase, Mol. Cell. Biochem. 264 (2004) 85–97.
[55] Y.-W. Kim, T.V. Byzova, Oxidative stress in angiogenesis and vascular disease, Blood 123 (2014) 625–631.
[56] T. Zhu, Q. Yao, W. Wang, H. Yao, J. Chao, iNOS induces vascular endothelial cell migration and apoptosis via autophagy in ischemia/reperfusion injury, Cell. Physiol. Biochem. 38 (2016) 1575–1588.
[57] A.Y. Kolyada, N.E. Madias, Transcriptional regulation of the human iNOS gene by IL-1β in endothelial cells, Mol. Med. 7 (2001) 329–343.
[58] A. Li, S. Dubey, M.L. Varney, R.K. Singh, Interleukin-8-induced proliferation, survival, and MMP production in CXCR1 and CXCR2 expressing human umbilical vein endothelial cells, Microvasc. Res. 64 (2002) 476–481.
[59] D.M. Radomska-Leśniewska, et al., N-acetylcysteine inhibits IL-8 and MMP-9 release and ICAM-1 expression by bronchoalveolar cells from interstitial lung disease patients, Pharmacol. Rep. 62 (2010) 131–138.
[60] A.M. Sadowska, B. Manuel-Y-Keenoy, W.A. De Backer, Antioxidant and anti-inflammatory efficacy of NAC in the treatment of COPD: discordant in vitro and in vivo dose-effects: a review, Pulm. Pharmacol. Ther. 20 (2007) 9–22.
[61] L.M. Schiffmann, et al., Mitochondrial respiration controls neoangiogenesis during wound healing and tumour growth, Nat. Commun. 11 (2020) 3653.
[62] S. Manandhar, S. Chambers, A. Miller, I. Ishii, M. Bhatia, Pharmacological inhibition and genetic deletion of cystathionine gamma-Lyase in mice protects against organ injury in Sepsis: a key role of adhesion molecules on endothelial cells, Int. J. Mol. Sci. 24 (2023) 13650.
[63] R. Wang, et al., The role of H2S bioavailability in endothelial dysfunction, Trends Pharmacol. Sci. 36 (2015) 568–578.
[64] T. Corsello, N. Komaravelli, A. Casola, Role of hydrogen sulfide in NRF2- and Sirtuin-dependent maintenance of cellular redox balance, Antioxidants 7 (2018) 129.
[65] B. Pang, et al., Emerging insights into the pathogenesis and therapeutic strategies for vascular endothelial injury-associated diseases: focus on mitochondrial dysfunction, Angiogenesis 27 (2024) 623–639.
[66] X. Zhang, H. Zhou, X. Chang, Involvement of mitochondrial dynamics and mitophagy in diabetic endothelial dysfunction and cardiac microvascular injury, Arch. Toxicol. 97 (2023) 3023–3035.